RNA Peach and Mango: orthogonal two-color fluorogenic aptamers distinguish nearly identical ligands

KRISTEN Y.S. KONG,[1] SUNNY C.Y. JENG,[1] BATOOL RAYYAN, and PETER J. UNRAU

Department of Molecular Biology and Biochemistry, Simon Fraser University, Burnaby, British Columbia V5A 1S6, Canada

ABSTRACT

Two-channel fluorogenic RNA aptamer-based imaging is currently challenging. While we have previously characterized the Mango series of aptamers that bind tightly and specifically to the green fluorophore TO1-Biotin, the next aim was to identify an effective fluorogenic aptamer partner for two-color imaging. A competitive in vitro selection for TO3-Biotin binding aptamers was performed resulting in the Peach I and II aptamers. Remarkably, given that the TO1-Biotin and TO3-Biotin heterocycles differ by only two bridging carbons, these new aptamers exhibit a marked preference for TO3-Biotin binding relative to the iM3 and Mango III A10U aptamers, which preferentially bind TO1-Biotin. Peach I, like Mango I and II, appears to contain a quadruplex core isolated by a GAA^A type tetraloop-like adaptor from its closing stem. Thermal melts of the Peach aptamers reveal that TO3-Biotin binding is cooperative, while TO1-Biotin binding is not, suggesting a unique and currently uncharacterized mode of ligand differentiation. Using only fluorescent measurements, the concentrations of Peach and Mango aptamers could be reliably determined in vitro. The utility of this orthogonal pair provides a possible route to in vivo two-color RNA imaging.

Keywords: RNA; Mango; Peach; TO1-B; TO3-B; orthogonal aptamers; two-color imaging

INTRODUCTION

Routine fluorescent based imaging of RNA has the potential to revolutionize RNA research as it would allow the direct imaging of RNAs within living cells. Until recently, the gold standard for in vivo RNA imaging involved the high affinity binding of MS2 coat protein (MCP) and MCP-fluorescent protein (FP) fusion constructs onto MS2 RNA tags that are incorporated into an RNA of interest (Bertrand et al. 1998). This MS2 system has been successfully diversified to a two-color imaging system by the use of the orthogonal MS2/PP7 system (Wu et al. 2014) fused to two distinct FPs (Hocine et al. 2013).

As an alternative to the MS2 and PP7 type systems, fluorogenic RNA aptamers that selectively bind and enhance the fluorescence of small molecule fluorophore ligands are now a rapidly expanding field of interest (Trachman and Ferré-D'Amaré 2019). We previously reported RNA Mango, a class of aptamers that bind tightly and enhance the fluorescence of thiazole orange-based fluorophores. RNA Mango has been used for various fluorescent imaging applications such as the in vivo tracking of RNA polymerase II and III transcripts as well as a central tool for in vitro fluorescence-based RNA technology (Dolgosheina et al. 2014; Autour et al. 2018; Trachman et al. 2018, 2019; Abdolahzadeh et al. 2019). Notably, live single molecule imaging of mRNA molecules using Mango II arrays has been achieved with significantly less background compared to the MS2 system (Cawte et al. 2020).

Using pairs of fluorogenic aptamers is in its infancy; RNA Mango and RNA Spinach (Paige et al. 2011) or its close relatives (Filonov et al. 2014; Song et al. 2017) have been used in the development of apta-FRET two channel imaging (Jepsen et al. 2018; Jeng et al. 2020). The Spinach family of aptamers, with its green ligand 3,5-difluoro-4-hydroxybenzylidene imidazolinone (DFHBI), have relatively weak fluorophore binding affinity and low ligand discrimination (Jeng et al. 2016), making the optimization of imaging conditions challenging. Variants of RNA Spinach, Orange/Red Broccoli, as well as RNA Corn have been developed to bind to a yellow analog of DFHBI, 3,5-difluoro-4-hydroxybenzylidene imidazolinone-2-oxime (DFHO). Unfortunately, the high spectral overlap between DFHBI and DFHO precludes their use as simultaneous orthogonal

[1]These authors contributed equally to this work.

Corresponding author: punrau@sfu.ca

Article is online at http://www.rnajournal.org/cgi/doi/10.1261/rna.078493.120.

tags (Filonov et al. 2014; Song et al. 2017). The recently selected Pepper aptamer is able to bind to a wide range of noncytotoxic cell permeable (4-((2-hydroxyethyl) (methyl)amino)-benzylidene)-cyanophenylacetonitrile (HBC) fluorophores with reported nanomolar affinity (Chen et al. 2019). It may have high ligand discrimination for fluorophores structurally dissimilar to HBC and its analogs, but this remains untested at this time. Further, the red fluorescent o-Coral aptamer with its nanomolar affinity to the noncytotoxic, cell permeable, self-quenching Gemini-561 fluorophore may also be a viable imaging partner (Bouhedda et al. 2020). However, the relatively long association time for o-Coral to Gemini-561 may pose a problem for time-dependent assays. Other fluorescent aptamers such as Riboglow with unique turn-on fluorescence mechanisms offer signals that span the visible light spectrum (Braselmann et al. 2018). However, the fluorophores required for this system are not cell permeable and may be bound by other cobalamin binding proteins within the cell.

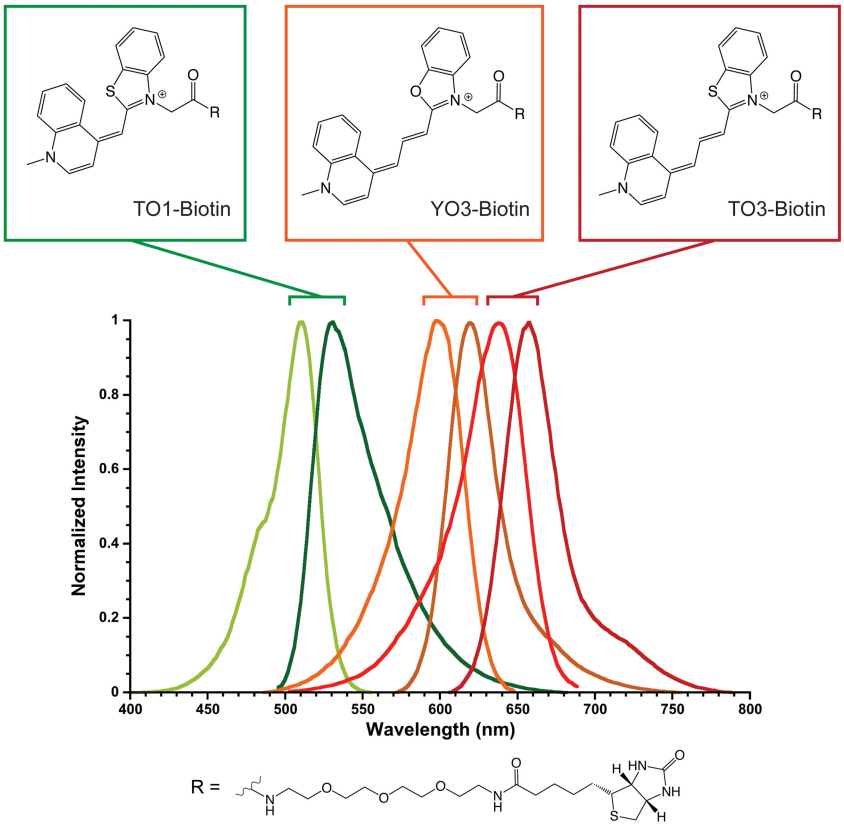

FIGURE 1. Excitation and emission scans of TO1-B, YO3-B, and TO3-B (0.4 µM) in excess RNA (1.5 µM). Spectra were measured with Mango III A10U bound to TO1-B and Peach I bound to either YO3-B or TO3-B. Lighter shading corresponds to excitation spectra, while the darker curves correspond to emission spectra for TO1-B (green), YO3-B (orange), and TO3-B (red).

The original RNA Mango series of aptamers (Autour et al. 2018) differentially bind to a series of thiazole-orange like ligands. Mango I, II and IV show little ability to differentiate between the closely related ligands TO1-Biotin (TO1-B, green channel, ex: 510 nm, em: 535 nm), YO3-Biotin (YO3-B, orange channel, ex: 595 nm, em: 620 nm) and TO3-Biotin (TO3-B, red channel, ex: 637 nm, em: 658 nm), binding all with nanomolar affinities and resulting in comparatively bright fluorescence (Dolgosheina et al. 2014; Jeng et al. 2016; Trachman et al. 2017; Autour et al. 2018; Jepsen et al. 2018). The lack of discrimination might be expected given the similarity of these ligands: TO3-B differing from TO1-B by only two sp^2 carbons that extend the methine bridge between the two heterocycles, while TO3-B and YO3-B differ by only a sulfur to oxygen atom substitution in the thiazole heterocycle (Fig. 1). Remarkably, however, the iM3 and Mango III A10U (MIII A10U) variants of Mango III have a distinct propensity to bind specifically to TO1-B (Trachman et al. 2019). We therefore sought to select for new aptamers able to preferentially bind TO3-B and not TO1-B so as to generate an orthogonal binding partner for the iM3 and MIII A10U series of aptamers.

We performed a competition-based in vitro selection for TO3-B binders, where aptamers able to bind TO1-B were disfavored. From this selection, two aptamers we call Peach I and Peach II were selected that favor binding to TO3-B. They bind TO3-B with nanomolar affinity and differentiate successfully between TO3-B and TO1-B despite the high similarity of these ligands. These aptamers have interesting features in common with the existing Mango aptamers, both being based on G-quadruplex cores and with Peach I having a GAA^A adaptor motif also found in the Mango I and II aptamers. In contrast to the Mango aptamers, the Peach aptamers show a cooperative binding response to TO3-B but not to TO1-B, indicating a novel and as yet uncharacterized binding mechanism to TO3-B. Together, we use the MIII A10U and Peach I aptamer pair to demonstrate robust in vitro quantification of RNA mixtures.

RESULTS

In vitro selection of RNA Peach aptamers

A competition-based in vitro selection was performed from an unbiased high diversity random sequence RNA

pool ($N = 87$, diversity of 10^{14}) to identify a red fluorescent TO3-B binding aptamer aversive to TO1-B binding. A total of 16 rounds were performed (Fig. 2) with each round using a combination of N-methyl mesoporphyrin IX (NMM, a general G-quadruplex binder), TO1-acetate, TO3-acetate, and various TO1 derivatives as competitor molecules in a physiological cell mimicking buffer (see Materials and Methods, Supplemental Table S1; Dolgosheina et al. 2014). In rounds three to five, free TO1-acetate was used as a competitor to help remove any nonspecific TO1 binders. In addition to this, free TO3-acetate was used to remove any fast off-rate aptamers, while NMM was used to reduce the accumulation of nonspecific G-quadruplex structures. Starting in round 6, TO1-propyl and TO1-methoxyethane were used as competitors to eliminate the negative charge within the carboxylate group of the acetate derivative as it might interfere with RNA binding (Supplemental Table S1). To promote the enrichment of fast on-rate binders, RNA binding time was decreased over each round of selection. To select TO3-B aptamers with a slow off-rate, competitor wash steps were performed using free TO3-acetate to compete for immobilized TO3-B binding. In order to eliminate aptamers that bound to competitors with a slow off-rate, preincubation steps with RNA in the presence of competitor molecules were done before binding to beads. Subsequent increases in wash times and competitor molecule concentrations provided further stringency. In rounds 12 and 13, mutagenic PCR (Cadwell and Joyce 1994) with a 0.66% mutation rate was performed to diversify the binding population still further.

Identification of potential Peach and Mango aptamer orthogonal pairs

RNA aptamers from rounds 12 and 15 of the RNA Peach pool were cloned and then introduced individually to a solution containing 100 nM TO1-B and 200 nM TO3-B. The signal intensity in the TO1-B and TO3-B fluorescence emission channels was then used to determine aptamers of interest (Supplemental Fig. S1) in order to identify

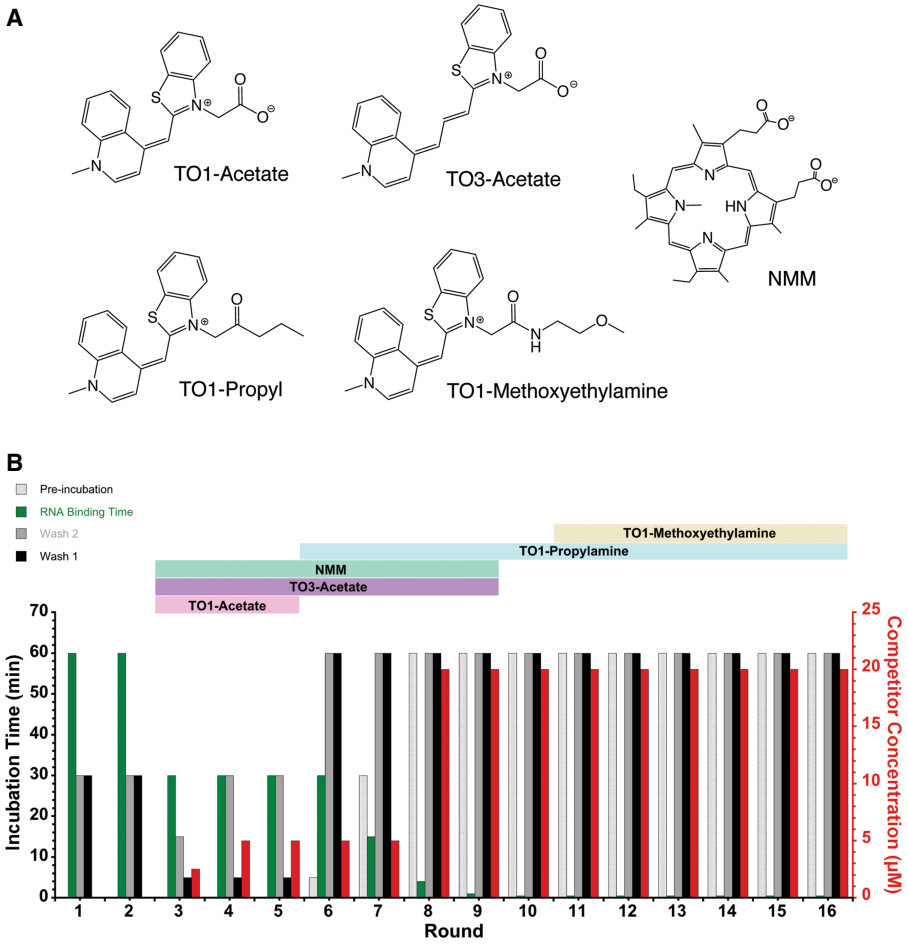

FIGURE 2. Competitive in vitro selection for TO3-B aptamers. (*A*) Chemical structures of the competitors in the TO3-B aptamer selection. (*B*) General scheme of the conditions for the 16 round TO3-B selection with indicated competitor molecules shown by the *horizontal* bars. Explicit competitor molecule details are found in Supplemental Table 1. The *left* axis depicts incubation times for preincubation, RNA binding, and wash 1 and 2 steps as indicated by the legend. The *right* axis indicates in red the competitor molecule concentration.

leading aptamers for further analysis. Aptamers R15-19 and R12-22 displayed the largest contrast being significantly brighter in the red channel than in the green channel (Supplemental Fig. S1). These two aptamers were therefore truncated to determine the minimal fully functional domain and resulted in Peach I (R15–19) and Peach II (R12–22). Peach I and II showed considerable contrast being 88-fold and 73-fold brighter in the red channel than in the green channel (Fig. 3). Of the existing Mango aptamers, MIII A10U had the highest green channel fluorescence and contrast between TO1-B and TO3-B channels being fivefold brighter in the green channel than in the red (Fig. 3).

The fluorescent properties of Peach I, II and MIII A10U were then characterized. Peach I and II bound 28- and 140-fold more weakly respectively to TO1-B than did MIII A10U, and when bound formed a complex with a final molar brightness nearly 10-fold less than for MIII A10U (Table 1; Supplemental Fig. S2). Peach I, which has a binding affinity to TO3-B of 19.6 ± 1.4 nM, exceeded that of MIII A10U and Peach II by approximately fourfold and achieved a final molar brightness twice that of MIII A10U, while Peach II was only 1.6-fold as bright. YO3-B was bound most tightly by Peach I, while Peach II bound 14-fold and MIII A10U bound fivefold weaker. Of note, the Peach I:YO3-B complex has a quantum yield of 0.84 and molar brightness of 77,300 $M^{-1}cm^{-1}$, making an exceptionally bright complex that exceeds the brightness of MIII A10U. This brightness, together with the spectral overlap between TO1-B and YO3-B (Fig. 1) may allow Peach I and Mango aptamers to be used as FRET pairs in the future.

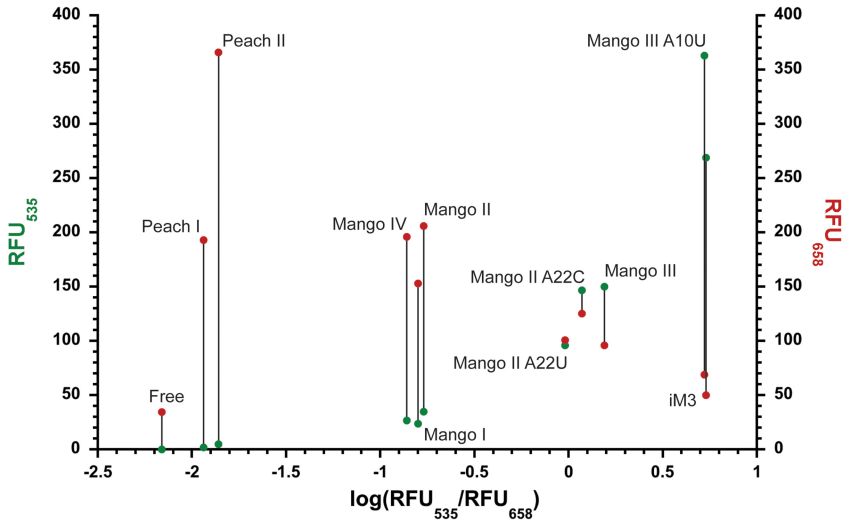

FIGURE 3. Relative and absolute fluorescence of the Peach and Mango aptamers. Aptamers from the Mango and Peach series (20 nM each) were incubated with 100 nM TO1-B and 200 nM TO3-B. Green dots indicate total fluorescence in the TO1-B channel (RFU_{535}), while red dots indicate total fluorescence in the TO3-B channel (RFU_{658}). Unbound TO1-B and TO3-B brightness is indicated by "Free."

While Peach I and II bind to TO3-B and YO3-B to form very bright complexes, the fluorescence enhancement for these complexes is comparatively low (Table 1). This results from the high fluorescence of the unbound TO3-B and YO3-B fluorophores relative to that of TO1-B, which is exceedingly dim when unbound. Titrating TO3-B while holding Peach I fixed resulted in data that were very well fit to a simple model, taking into account the linear increase in fluorescence expected from unbound fluorophore superimposed on a single ligand binding model (Supplemental Fig. S3). The resulting K_D agreed with the previous titration data (Table 1), while Peach II showed evidence of a more complex binding behavior, perhaps involving two binding events. This anomalous behavior of Peach II focused our attention increasingly on Peach I as the brightest most useful aptamer of the pair.

Peach aptamers bind TO3-B cooperatively but not with TO1-B

Unexpectedly, fluorescence melting curves for Peach aptamers indicated that both aptamers cooperatively bind the TO3-B ligand but not the TO1-B ligand. Peach I, which binds TO3-B most tightly, had a strong sigmoidal-like rate of change in fluorescent melting signal, which peaked at 56°C, but exhibited only a weak linear increase in fluorescent rate of change when binding TO1-B (Fig. 4A). Peach II, which binds TO3-B threefold more weakly than Peach I, exhibited similar sigmoidal melting behavior and exhibited a maximum rate of change in fluorescence at 51°C. Peach II, in contrast to Peach I, showed a small step-like increase in fluorescent rate of change when melting with the TO1-B ligand. As with the TO3-B ligand, this step occurs at the same approximate melting temperature suggesting that a common nucleic acid structure independent of TO1-B and TO3-B binding melts at this temperature (Fig. 4B). MIII A10U, in contrast to both Peach I and II, showed strong sigmoidal-like melting with TO1-B ligand having a maximal rate of change at 48°C. A weak sigmoidal-like melting transition was observed with TO3-B and at a significantly lower temperature of 34°C (Fig. 4C) than any of the other melting transitions observed in this study.

Peach I and II tertiary structures

Planar G-quadruplex structures provide an ideal surface for the binding of TO1-B in Mango I, II, III, and IV (Dolgosheina et al. 2014; Trachman et al.

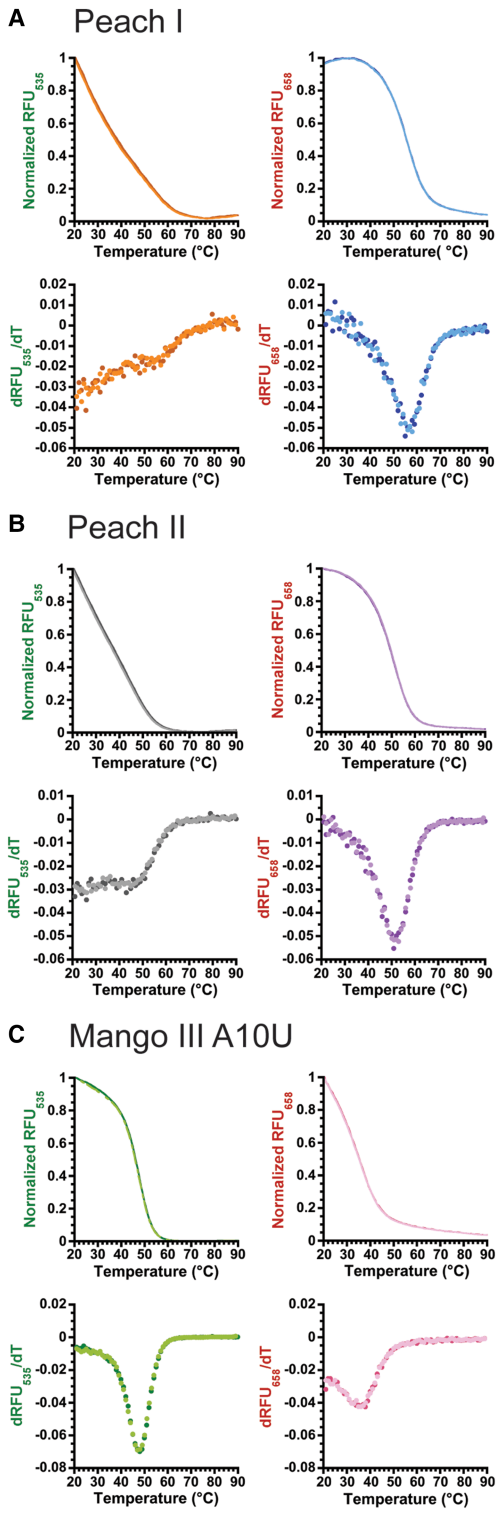

FIGURE 4. Melting curves of Peach and Mango Aptamers (200 nM) in the presence of excess (2 µM) TO1-B (*left*) or TO3-B (*right*). (*A*) Peach I, (*B*) Peach II, and (*C*) MIII A10U. Simple derivatives of each melting curve are plotted *underneath* each fluorescent melting curve. Darker colors represent data from increasing temperature ramps, while lighter colors represent data from deceasing temperature ramps. A ramp rate of 1°C/min starting at 90°C and moving to 20°C, and returning to 90°C was used.

2017, 2018, 2019, 2020). All Mango aptamers stack their TO1-B ligand onto an adjacent G-quadruplex tetrad with coplanarity between these heterocycles being an important characteristic for high quantum yield (Trachman et al. 2017, 2018, 2019). We hypothesized that the G-rich sequences of Peach I and Peach II (46% G and 40% G, respectively) also contained G-quadruplex motifs (Fig. 5A). G-quadruplex structures are stabilized by monovalent salts such as potassium and, to a lesser extent, sodium (Lane et al. 2008). Ions more readily hydrated, such as lithium, are unable to stabilize complete G-quadruplex structures due to a combination of size and hydration energy (Hud et al. 1996; Gu and Leszczynski 2002). Therefore, titrations using these cations were performed to probe for the presence of G-quadruplex motifs in the presence of either TO1-B or TO3-B ligands. As expected, titration with lithium or sodium ions did not elicit a significant fluorescent response, while potassium gave a strong fluorescent enhancement for both aptamers and fluorophores. Hill coefficients in the presence of TO3-B for potassium ions were found to be 1.7 ± 0.2 and 1.6 ± 0.1 for Peach I and II, respectively, (Table 2; Supplemental Fig. S4). In the presence of TO1-B, Hill coefficients were slightly lower with values of 1.5 ± 0.1 and 1.4 ± 0.1 for Peach I and II, respectively (Table 2; Supplemental Fig. S4). When folded in the presence of lithium ions no fluorescence activation was observed, suggesting that both aptamers use G-quadruplexes as structural elements (Supplemental Fig. S4).

Like Mango I (Dolgosheina et al. 2014), the Peach aptamers are sensitive to high levels of magnesium as indicated by a loss in fluorescence observed with increasing millimolar concentrations of $MgCl_2$ (Supplemental Fig. S5). This may indicate a propensity for the Peach aptamers to misfold at high divalent metal ion concentrations, which can pose a problem for high magnesium in vitro applications. In contrast, Mango II, III, and IV, are substantially magnesium resistant (Autour et al. 2018) as are the Spinach-family aptamers which exhibit increased fluorescence at higher magnesium conditions (Filonov et al. 2014).

To obtain more direct evidence of the quadruplex nature of the Peach aptamer structures, DMS probing was then performed. A clear protection pattern of eight G residues was observed for Peach I, consistent with a well ordered two-tiered G-quadruplex (Fig. 5A; Supplemental Fig. S6). Even with a twofold shorter DMS modification step as compared to Peach I, Peach II exhibited little guanine protection (Supplemental Fig. S6). This suggests, in our opinion, an aptamer that can fold into multiple nearly equivalent ligand bound structures, which is consistent with our melting curve and titration data.

Peach I contains a GAA^A tetraloop-like adaptor

Like Mango I and II, Peach I appears to contain a flexible GAA^A tetraloop-like junction motif that isolates the

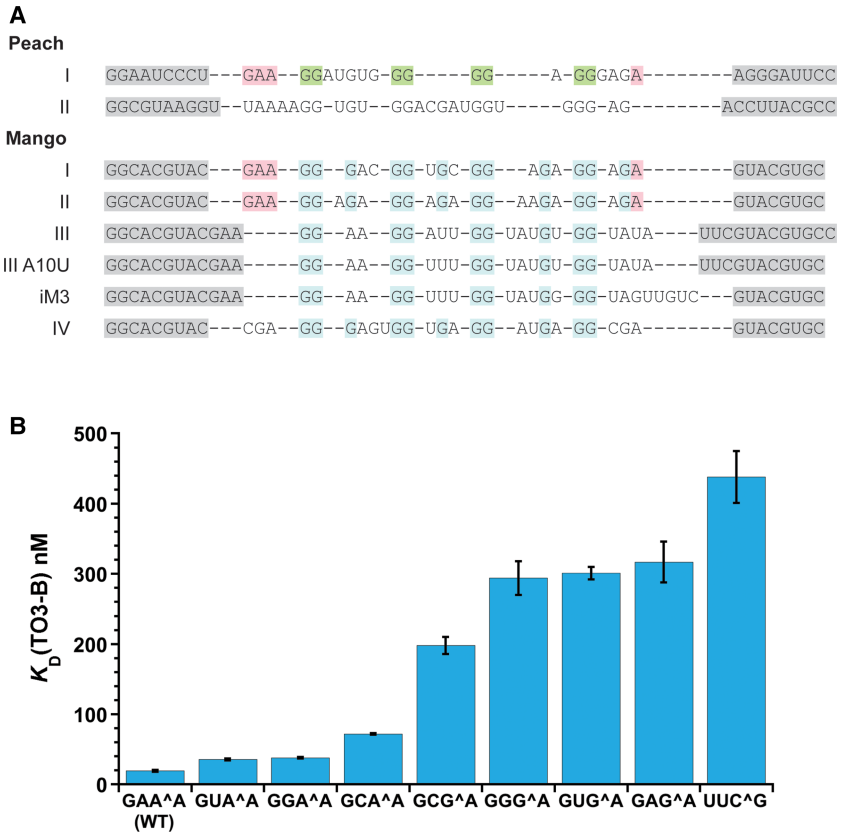

FIGURE 5. Effects of binding affinity by mutations in the Peach I GAA^A tetraloop-like motif. (*A*) Aligned sequences of Peach and Mango fluorogenic aptamers. For Peach I, G-residues predicted to participate in a G-quadruplex formation based on DMS probing data are shown in green. For Mango, G residues involved in quadruplex formation as determined by crystal structure are shown in blue. Stem regions are in gray, while GAA^A tetraloop motifs are indicated in pink. (*B*) Binding affinity measurements were performed testing the eight possible GNR^A type junction motifs in Peach I together with a potential UUC^G type motif.

quadruplex core of the aptamer from an exterior closing stem (Fig. 5A). This motif interrupts a standard GNRA tetraloop by inserting the quadruplex core of the aptamer, denoted by the symbol "^", between the third and fourth positions of the loop. GAA^A was found to be the optimal motif followed closely by GUA^A and GGA^A, then GCA^A (Fig. 5B). This GNA^A pattern is shared in common with Mango I, where the second position was also found not to play a significant role in destabilizing aptamer function, so long as the third position was an A (Trachman et al. 2017). As with Mango I, the GNG^A series of junction motifs were substantially destabilizing when tested on Peach I; with GGG^A, GUG^A and GAG^A having substantially weaker binding and GCG^A showing intermediate binding. Consistent with Peach I having a GAA^A like junction motif, placing an otherwise stable UUC^G loop (Antao et al. 1991) into the GAA^A Peach I motif sequence context resulted in substantially destabilized binding.

In vitro quantification using the Peach I and MIII A10U orthogonal fluorogenic aptamers

To determine if it was possible to quantify two RNA concentrations simultaneously using only the fluorescence resulting from MIII A10U and Peach I, both aptamers were titrated over various concentration gradients ranging from 0 to 50 nM using 100 nM of both TO1-B and TO3-B in WB buffer. For each mixture, the red and green channels (Materials and Methods) were read. No fluorescent signal correction was required as there was no bleed-through observed between the red and green channels (Supplemental Fig. S7). A simple linear binding model defined by a four-parameter fit (one intercept and slope for each color channel, Table 3) fit all four independent titrations shown in Figure 6 simultaneously, with the data deviating from this fit only at the higher Peach I concentrations tested (Fig. 6C,D; Supplemental Fig. S8).

To determine if RNA concentrations could be recovered de novo from fluorescence measurements, six samples containing arbitrary mixtures of RNA concentrations were prepared by a third party and introduced to the same 100 nM equimolar mixture of dyes and WB buffer. Using the linear parameters determined in Table 3 (and that are specific to our spectrometer), the unknown aptamer concentrations were determined with an average deviation of only 7% (Table 4; Fig. 6E).

DISCUSSION

Here, two RNA Peach fluorogenic aptamers have been identified through in vitro selection and subsequently characterized. Similar to fluorogenic aptamers that precede them, such as RNA Mango and RNA Spinach (Paige et al. 2011; Dolgosheina et al. 2014), the Peach aptamers likely contain G-quadruplex cores as indicated by metal ion titration (Lane et al. 2008). In the case of Peach I, the DMS protection of eight guanine residues indicates the presence of a G-quadruplex structure containing at least two G quartets. While most RNA Mango aptamers contain three tier G-quadruplexes, two tier quadruplexes have also been found as stable motifs such as in the Mango III aptamer (Trachman et al. 2017, 2018, 2019, 2020; Autour et al.

TABLE 1. RNA aptamer fluorophore complex binding affinity and brightness properties for Peach I, II, and MIII A10U

	Aptamer type		
	Peach I	Peach II	MIII A10U
Bound properties			
K_D(TO1-B) (nM)	43 ± 4	216 ± 14.5	**1.5 ± 0.1**[a]
Molar brightness (aptamer: TO1-B)	4350 ± 300	5480 ± 410	**41,600 ± 2520**
$\phi_{Aptamer:TO1-B}$	0.07 ± 0.01	0.09 ± 0.01	**0.66 ± 0.04**[b]
F_E(TO1-B)	542 ± 17.5	683 ± 30.0	**5185**[b]
$F_{efficiency}$	12.6	3.2	**3500**
K_D(TO3-B) (nM)	**19.6 ± 1.4**	**71 ± 5.6**	78 ± 7.0
Molar brightness (aptamer: TO3-B)	**17,800 ± 2000**	**12,900 ± 1540**	8040 ± 1000
$\phi_{Aptamer:TO3-B}$	**0.27 ± 0.03**	**0.19 ± 0.02**	0.12 ± 0.01
F_E(TO3-B)	**50 ± 2**	**37 ± 1**	23 ± 1
$F_{efficiency}$	**2.5**	**1.9**	0.29
K_D(YO3-B) (nM)	22 ± 0.6	190 ± 12	118 ± 7
Molar brightness (aptamer: YO3-B)	77,300 ± 7360	54,400 ± 5680	47,600 ± 4850
$\phi_{Aptamer:YO3-B}$	0.8 ± 0.1	0.6 ± 0.1	0.5 ± 0.1
F_E(YO3-B)	130 ± 3	92 ± 4	80 ± 3
$F_{efficiency}$	5.9	0.48	0.68

Fluorescent enhancement (F_E) of emission measured between bound and free fluorophore ligand. $F_{efficiency}$ is defined by F_E/K_D. Bolded column values reflect aptamer-fluorophore pairs that were optimized directly by in vitro selection and/or design.
[a]Calculated with a three-parameter fit.
[b]Trachman et al. 2019.

2018). Interestingly, Peach I uses a GAA^A type motif to isolate its core binding motif from its external sequence, similar to that found previously for Mango I and Mango II aptamers (Trachman et al. 2017, 2018).

The importance of isolating a G-quadruplex core from external sequence by a GAA^A type motif to ensure correct aptamer folding is unexpected but has been seen now in two independent in vitro selections. This suggests that functional G-quadruplexes in nature may also use such a strategy, and bioinformatics searches should be performed to uncover any evidence of this hypothesis in nature.

A fluorogenic aptamer can differentiate between similar fluorogenic ligands by two distinct processes: namely recognizing each ligand with distinct affinities (K_D values) and/or by producing a distinct fluorescent response upon binding (fluorescence enhancement or F_E). The ratio of these two numbers defines a performance metric called the fluorescence efficiency: $F_{efficiency} = F_E/K_D$ (Dolgosheina et al. 2014). By this metric, MIII A10U is outstanding with an efficiency of 3500 for TO1-B binding, while Peach aptamers are more than 10-fold less efficient when binding the TO1-B fluorogenic ligand. Such high differential efficiencies result from a combination of decreased binding affinities and fluorescence enhancements for the Peach aptamers.

Unbound TO3-B is much brighter than TO1-B and thus fluorescence enhancements and efficiencies for the Peach aptamers are correspondingly lower. Peach I is however 8.6-fold more fluorescently efficient when binding TO3-B than MIII A10U and 8.7-fold more efficient with YO3-B. Peach II was uniformly less effective by this metric relative to Peach I. Thus, and as this aptamer is much less well behaved, Peach I and MIII A10U are predicted to be the best fluorogenic pair for orthogonal two channel imaging, having significant resolution between the red and green color channels as shown in Figures 3, 6 and Table 1.

Structural studies of the Mango aptamers have revealed a range of binding mechanisms to the TO1-B ligand. All Mango aptamers (I, II, III and IV) crystallized to date involve the stacking of the TO1-B heterocycles over the top of a

TABLE 2. Hill coefficients of potassium for Peach I and II

Aptamer	Fluorophore	Hill coefficient	$K_D(K^+)$ mM
Peach I	TO3-B	1.7 ± 0.2	9.5 ± 1
	TO1-B	1.5 ± 0.1	15 ± 1
Peach II	TO3-B	1.6 ± 0.1	10 ± 1
	TO1-B	1.4 ± 0.1	14 ± 1

TABLE 3. Linear fits of Mango Peach aptamer gradients determined from Figure 6A–D

RNA gradient	RFU_{535} slope (green channel)	RFU_{535} intercept (red channel)	RFU_{658} slope (red channel)	RFU_{658} intercept (red channel)
Peach I	-	-	8.0 ± 0.1	30.2 ± 3.9
MIII A10U	15.0 ± 0.1	16.8 ± 2.7	-	-

These fits are dependent on the fluorometer being used.

quadruplex binding face by van der Waals interactions, but each aptamer type differs significantly as to how this basic geometry is further stabilized. Mango I, for example, positions two adenine residues over each heterocycle of TO1-B and shows no strong ability to differentiate TO1-B binding from TO3-B (Fig. 3; Trachman et al. 2017). Mango II, which forms a stadium-like array of adenine residues around its ligand binding pocket, also differentiates very poorly between TO1-B and TO3-B and is known to exhibit heterogeneous binding (Trachman et al. 2018). Mango III, which positions a trans A:A base pair over its TO1-B ligand only becomes strongly discriminating against TO3-B when this pair becomes A:U, as was found in the MIII A10U and iM3 mutants (Fig. 3; Trachman et al. 2019). This discrimination appears to result from the precise positioning of the TO1 heterocycles with respect to not only the A:U pair and the G-quadruplex, but also with respect to a uridine base found nearly perpendicular to the methine carbon of TO1-B. When TO1-B is replaced with TO3-B or YO3-B, all such interactions are presumably destabilized resulting in the high discrimination observed for these mutants of Mango III.

How might Peach I differentiate between TO3-B and TO1-B? Both appear to form quadruplex structures and we speculate that just as for the Mango aptamers, TO3-B is likely to stack on a quadruplex face. As for Mango I and III, we propose that unique nucleic acid structures exist to sandwich this fluorophore into a binding pocket in a cooperative

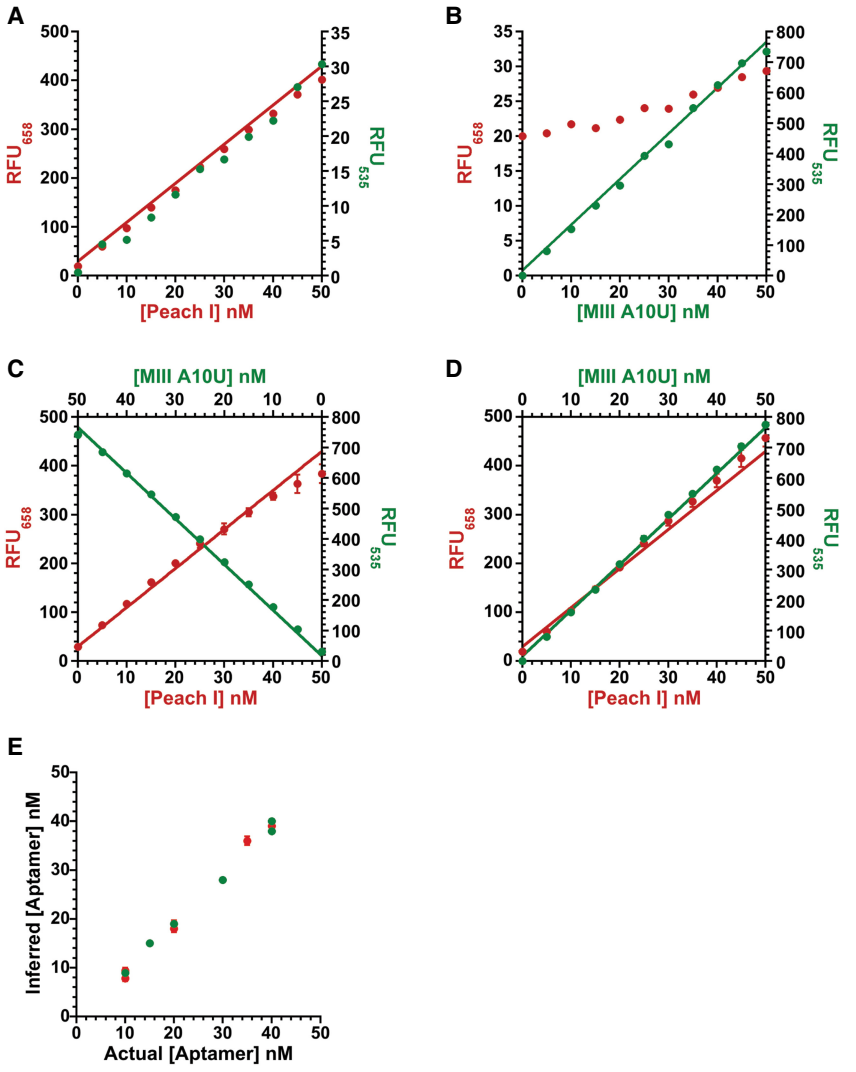

FIGURE 6. RNA aptamer gradients with Peach I and MIII A10U in the presence of 100 nM TO1-B and 100 nM TO3-B. Fluorescent signals from singly titrated aptamers for (*A*) Peach I and (*B*) MIII A10U as well as from simultaneous aptamer gradients with (*C*) increasing Peach I and decreasing MIII A10U (*D*) for both increasing Peach I and MIII A10U over a range of 0 to 50 nM RNA. Fits were weighted with triplicate readings of simultaneous gradients (*C*,*D*) and a singlet reading of single aptamer gradients (*A*,*B*). (*E*) In a blinded study, the correlation between the actual and inferred aptamer concentrations shown in Table 4 is plotted. Concentrations of Peach I (red) and MIII A10U (green) in samples A to F were quantified from fits in *A*–*D* and Table 3.

TABLE 4. Blind orthogonal aptamer quantification

	Concentration (nM) inferred from Mango Peach fluorescence		Actual concentrations (nM)		Percent discrepancy	
Sample	(Peach I)	(MIII A10U)	(Peach I)	(MIII A10U)	Peach I	MIII A10U
A	9.4 ± 0.6	38 ± 0.4	10	40	−5.8%	−6.3%
B	19 ± 0.7	28 ± 0.4	20	30	−5.6%	−6.3%
C	36 ± 0.9	15 ± 0.3	35	15	+1.6%	+0.7%
D	7.8 ± 0.6	8.9 ± 0.2	10	10	−22%	−11%
E	18 ± 0.7	19 ± 0.3	20	20	−11%	−4.9%
F	39 ± 1.0	40 ± 0.4	40	40	−3.5%	−1.1%

Concentrations corresponding to samples A to F were inferred from fits to the data shown in Figure 6 and summarized in Table 3. These calculated values were then compared to the actual RNA concentrations used in each experiment.

fashion where the fluorophore first binds and then in a second step, a nucleic acid structure assembles so as to further constrain the ligand. This point of view is supported by our melting curve titrations, but a detailed understanding of this discrimination and the mechanism of fluorescent enhancement will need to await further structural characterization of these fluorogenic Peach aptamers. Together with Mango aptamers, they offer in vitro and potentially in vivo two-color RNA imaging solutions.

MATERIALS AND METHODS

Conventional PCR

Conventional PCR reactions were performed using *Taq* polymerase (NEB) in *Taq* buffer (NEB), dNTPs (0.2 mM each), as well as forward and reverse primers (0.1 µM each, IDT). The following three step cycle was used: 94°C for 45 sec, 52°C for 1 min 25 sec, and 72°C for 1 min 55 sec. A pilot PCR was done to determine the optimal number of cycles.

Reverse-transcription PCR

Duplex DNA was regenerated from pool RNA after each round of selection using RT-PCR. RNA was reverse transcribed using Maxima RT enzyme (Thermo Fisher) in the provided RT buffer, 0.5 mM dNTPs, 1 µM RT primer, 0.01 M DTT, and 20 U/µL of Maxima enzyme. The RT-mix was preincubated at 65°C before adding enzyme and incubating at 50°C for 1 h. The reaction was then base-treated in 0.1 M KOH, with 0.5 µM final forward and reverse primer concentrations, at 90°C for 15 min. The reaction was then neutralized using 0.5 M Tris-HCl to a final pH of 7 before diluting fivefold into PCR reaction conditions. A reaction was done in parallel with no RT enzyme added as a negative control. The RT reaction was amplified by PCR using *Taq* polymerase (NEB). A pilot reaction was done with + and – RT to determine the number of optimal PCR cycles.

Mutagenic PCR

To perform mutagenic PCR after reverse transcription reaction, we adapted a previously established protocol (Cadwell and Joyce 1994). *Taq* polymerase was used as in standard PCR, with the addition of 5.5 mM $MgCl_2$ and 0.5 mM $MnCl_2$. The dNTP mixed was adjusted to 2 mM dGTP, 2 mM dATP, 10 mM dCTP, and 10 mM dTTP.

Transcription and purification of RNA

RNA was transcribed in vitro by combining T7 buffer (40 mM TRIS buffer pH 7.9, 2.5 mM spermidine, 26 mM $MgCl_2$, 0.01% Triton X-100), NTPs (8 mM GTP, 5 mM CTP, 5 mM ATP, 2 mM UTP), 10 mM DTT, 1 U/µL T7 RNA polymerase (abm), and 1 µM DNA template (IDT or 2× PCR product). The mixture was incubated for 1.5 h at 37°C. Afterward, the reaction was stopped and RNA denaturing loading dye (49% formamide, 0.5 mM EDTA, 0.0125% xylene cyanol, and 0.0125% bromophenol blue) was added followed by heating to 90°C. The transcription products were run on 8% PAGE (19:1 Acrylamide:bis). RNA bands were visualized by UV shadowing, cut out, and left to elute overnight in 300 mM NaCl at 4°C on a rotator. The RNA was then ethanol precipitated, the pellet resuspended in ddH_2O and stored at −20°C.

In vitro selection of RNA Peach aptamers

From an initial DNA pool, RNA was generated by in vitro transcription and introduced to TO3-B anchored to magnetic streptavidin beads and washed with a succession of competitor molecules (Supplemental Table S1). Bound RNA was isolated by heat denaturation in 95% formamide and 50 mM EDTA. The isolated RNA was reverse transcribed and amplified by PCR. Rounds of selection were performed in in vivo mimicking wash buffer (WB) containing 10 mM NaH_2PO_4 pH 7.2, 140 mM KCl, 1 mM $MgCl_2$, and 0.05% Tween-20.

Fluorescence spectroscopy

From in vitro transcription, RNA concentrations were determined by measuring absorbance at 260 nm in ddH_2O on a Nanodrop One C (Thermo Scientific). Molar extinction coefficients were calculated using the nearest neighbor method (Cavaluzzi and Borer 2004). Similarly, fluorophore concentrations were calculated by measuring absorbance in ddH_2O and using the following extinction coefficients: $\varepsilon_{500} = 63{,}000\ M^{-1}cm^{-1}$, $\varepsilon_{580} = 92{,}000\ M^{-1}cm^{-1}$, and $\varepsilon_{615} = 66{,}800\ M^{-1}cm^{-1}$ for TO1-B, YO3-B, and TO3-B, respectively.

All fluorescent measurements were taken using a Varian Cary Eclipse spectrophotometer; excitation and emissions were set at 510/535 nm, 595/620 nm, or 637/658 nm for TO1-B, YO3-B, or TO3-B. Readings were taken with a 5 mm excitation slit and a 10 mm emission slit.

Spectral scans were recorded for the excitation and emission of bound dye (0.4 µM) TO1-B, YO3-B, and TO3-B in WB buffer in the presence of excess RNA (1.5 µM). For TO1-B, MIII A10U RNA was used, while Peach I was used for YO3-B and TO3-B. Prior to taking readings, samples were incubated at room temperature for at least 1 h.

To determine K_D and fluorescent enhancement, fluorescent titration measurements were performed in WB buffer in the presence of 10 nM of dye. The resulting curves were fitted by least-squares according to either one of the two equations below using a nonlinear regression analysis (Kaleidagraph 4.5) and are called the three and two parameter fit, respectively:

$$F = F_{dye} + \frac{F_{complex} - F_{dye}}{2}(K_D + [RNA] + [dye] - \sqrt{([RNA] - [dye])^2 + K_D\,(K_D + 2[RNA] + 2[dye])}) \quad (1)$$

or

$$F = F_{dye} + \frac{(F_{complex} - F_{dye})[RNA]}{K_D + [RNA]}, \quad (2)$$

and as indicated at the bottom of Table 1, where F is the fluorescence at a given aptamer concentration [*RNA*], F_{dye} is fluorescence of unbound dye, $F_{complex}$ is the maximum fluorescence of complex when all dye is bound, and [dye] corresponds to TO1-B, YO3-B, or TO3-B concentration when applicable. Fluorescent enhancement was calculated using the following equation for RNA complexes with TO3-B or YO3-B:

$$F_E = \frac{F_{complex}}{F_{dye}}, \quad (3)$$

while RNA complexes with TO1-B for Peach I and II were calculated using:

$$F_{max}(RNA{:}TO1\text{-}B) = \frac{F_E(RNA{:}TO1\text{-}B)}{F_E(MIII\ A10U{:}TO1\text{-}B)} \times F_{max}(MIII\ A10U{:}TO1\text{-}B), \quad (4)$$

where F_{max} for corresponding RNA:TO1-B complexes is calculated from the two or three parameter fit, and F_E(MIII A10U:TO1-B) was assumed to be 5185 (Trachman et al. 2019).

Molar brightness was determined as a product of extinction coefficient and quantum yield with bound dye. Extinction coefficients of the dyes listed above were used as there is little change compared to bound and unbound dye (Supplemental Fig. S9). Quantum yield of Peach I was determined with either TO3-B or YO3-B by comparing with a Cy5 standard according to the following equation:

$$\phi_{PI:Dye} = \frac{m_{PI:Dye}}{m_{Cy5}} \times \frac{mol_{Cy5}}{mol_{PI:Dye}} \times \phi_{Cy5}, \quad (5)$$

where m is the slope of area under the emission curve at a given wavelength with either PI in complex with TO3-B/YO3-B or Cy5. The moles (mol) of Cy5 and PI in complex with TO3-B/YO3-B were also taken into account. Samples were initially normalized to an absorbance of 0.01, and ϕ_{Cy5} was assumed to be 0.27 (Mujumdar et al. 1993).

Quantum yield of PII and MIII A10U bound to either TO3-B or YO3-B was then determined using a ratiometric calculation with the following equation:

$$\phi_{RNA:Dye} = \frac{\phi_{PI:Dye}}{\text{RFU per nM complex}_{PI:Dye}} \times \text{RFU per nM complex}_{RNA:Dye}, \quad (6)$$

where RFU per nM complex was determined with the one-to-one binding model above using either Equation 1 or Equation 2 as indicated in Table 1.

PI/PII:TO1-B values were determined using a similar method where quantum yield was calculated as a product of the extinction coefficient (77,500) and the quantum yield (0.66 ± 0.04) of MIII A10U (Trachman et al. 2019) and then used as a comparison in a ratiometric calculation.

To determine the Hill coefficient, monovalent salt titration measurements for Li^+, Na^+, and K^+ were done in Tris buffer (10 mM, pH 7) containing Tween-20 (0.05%), $MgCl_2$ (1 mM), and TO3-B (100 nM). The resulting data were fitted to the following Hill equation using a nonlinear regression analysis (Kaleidagraph 4.5):

$$F = F_0 + \frac{F_{max}[TO3 - B]^h}{K_D^h + [TO3 - B]^h}, \quad (7)$$

where F is fluorescence given at [salt], F_0 is fluorescence of unbound dye, F_{max} is the maximum fluorescence, and *h* is the Hill coefficient. Magnesium titrations were done in a similar fashion.

Melting curves were performed with Peach I, Peach II, or MIII A10U aptamers at a 200 nM concentration with 2 µM of TO1-B or TO3-B in WB buffer. Samples were first heated to 90°C before reading fluorescence. Samples were read from 90°C to 20°C, then back to 90°C with a change of temperature at a rate of 1°C per minute. Simple derivatives were plotted by finding the slope at data point "t" by the following equation:

$$Slope_t = \frac{(Y_{t+1} - Y_{t-1})}{(X_{t+1} - X_{t-1})}, \quad (8)$$

where Y is the normalized fluorescence and X is temperature (°C).

For the quantification of RNA based on fluorescence, RNA gradient mixtures were prepared in WB buffer, TO1-B (100 nM), and TO3-B (100 nM) and incubated at room temperature for at least 30 min prior to readings. Blinded RNA samples were prepared by a laboratory member (S. Saeidiborojeni) and then tested by K. Kong. RNA concentrations were determined as described above. Fluorescence concentration determinations were performed by measuring obtained RFU_{535} and RFU_{658} values from

each blinded sample were interpolated onto the relationship derived from the RNA gradients. Linear fits were fitted to the data with Kaleidagraph 4.5.

DMS probing

DMS protocol was adapted from Lorsch and Szostak (1994). For denaturing DMS, gel purified RNA was 3′ end labeled with ^{32}P cytidine 3′–5′ bisphosphate (pCp). This RNA was incubated at 50 nM in 50 mM HEPES pH 7.5 at RT for 30 min, carrier DNA (7.5 µM) and diluted dimethyl sulfate (DMS, 0.125% final, diluted in ethanol, Sigma Aldrich) was added and the sample heated to 80°C for 2 min. To stop the reaction, the sample was ethanol precipitated. For native DMS, 3′ end labeled RNA (50 nM) was incubated in 50 mM HEPES pH 7.5, 140 mM KCl, and with or without 1 µM TO3-B or TO1-B at RT for 30 min. Afterwards, carrier DNA (7.5 µM) was added, and the sample was incubated as RT with DMS (1% final). DMS was left to react for 15 min for Peach I and 7 min for Peach II. Once again, the reaction was stopped by ethanol precipitation. Beyond this point, all samples were treated the same. For the reduction step, the pellets were first suspended in Tris buffer (1 M, pH 8) and $NaBH_4$ (0.1 M, freshly prepared in ddH_2O) was then added. The reaction was incubated on ice in the dark for 30 min and stopped by ethanol precipitation. For aniline cleavage, the pellet was suspended in an aqueous solution consisting of aniline (1 M, Sigma Aldrich) and acetic acid (4.8 M, Sigma Aldrich) and incubated at 60°C in the dark for 15 min. Samples were flash frozen and lyophilized by a speed vacuum centrifuge. Afterwards, the pellets were suspended in 20 µL ddH_2O, flash frozen, and lyophilized again. Pellets were resuspended in denaturing loading dye prior to running on a 10% PAGE (19:1 Acrylamide:bis).

T1 RNase ladder and alkaline hydrolysis ladder

For the T1 RNase ladder, 3′ end labeled RNA was first incubated in sodium citrate (20 mM, pH 8.5), urea (6.3 M), and T1 RNase (16 U/µL, Thermo Scientific) at 50°C for 12 min, flash frozen and then heated to 95°C for 5 min immediately before gel loading. For the hydrolysis ladder, 3′ end labeled RNA was incubated in $NaHCO_3$ (50 mM) at 90°C for 25 min and subsequently neutralized with Tris-HCl (50 mM).

SUPPLEMENTAL MATERIAL

Supplemental material is available for this article.

ACKNOWLEDGMENTS

This work was supported by the Natural Sciences and Engineering Research Council of Canada.

Received November 27, 2020; accepted February 25, 2021.

REFERENCES

Abdolahzadeh A, Dolgosheina EV, Unrau PJ. 2019. RNA detection with high specificity and sensitivity using nested fluorogenic Mango NASBA. *RNA* **25:** 1806–1813. doi:10.1261/rna.072629.119

Antao VP, Lai SY, Tinoco I. 1991. A thermodynamic study of unusually stable RNA and DNA hairpins. *Nucleic Acids Res* **19:** 5901–5905. doi:10.1093/nar/19.21.5901

Autour A, Jeng SCY, Cawte A D, Abdolahzadeh A, Galli A, Panchapakesan SSS, Rueda D, Ryckelynck M, Unrau PJ. 2018. Fluorogenic RNA Mango aptamers for imaging small non-coding RNAs in mammalian cells. *Nat Commun* **9:** 1–12. doi:10.1038/s41467-018-02993-8

Bertrand E, Chartrand P, Schaefer M, Shenoy SM, Singer RH, Long RM. 1998. Localization of ASH1 mRNA particles in living yeast. *Mol Cell* **2:** 437–445. doi:10.1016/S1097-2765(00)80143-4

Bouhedda F, Fam KT, Collot M, Autour A, Marzi S, Klymchenko A, Ryckelynck M. 2020. A dimerization-based fluorogenic dye-aptamer module for RNA imaging in live cells. *Nat Chem Biol* **16:** 69–76. doi:10.1038/s41589-019-0381-8

Braselmann E, Wierzba AJ, Polaski JT, Chromiński M, Holmes ZE, Hung S-T, Batan D, Wheeler JR, Parker R, Jimenez R, et al. 2018. A multicolor riboswitch-based platform for imaging of RNA in live mammalian cells. *Nat Chem Biol* **14:** 964–971. doi:10.1038/s41589-018-0103-7

Cadwell RC, Joyce GF. 1994. Mutagenic PCR. *Genome Res* **3:** S136–S140. doi:10.1101/gr.3.6.S136

Cavaluzzi MJ, Borer PN. 2004. Revised UV extinction coefficients for nucleoside-5′-monophosphates and unpaired DNA and RNA. *Nucleic Acids Res* **32:** e13. doi:10.1093/nar/gnh015

Cawte AD, Unrau PJ, Rueda DS. 2020. Live cell imaging of single RNA molecules with fluorogenic Mango II arrays. *Nat Commun* **11:** 1–11. doi:10.1038/s41467-020-14932-7

Chen X, Zhang D, Su N, Bao B, Xie X, Zuo F, Yang L, Wang H, Jiang L, Lin Q, et al. 2019. Visualizing RNA dynamics in live cells with bright and stable fluorescent RNAs. *Nat Biotechnol* **37:** 1287–1293. doi:10.1038/s41587-019-0249-1

Dolgosheina EV, Jeng SCY, Panchapakesan SSS, Cojocaru R, Chen PSK, Wilson PD, Hawkins N, Wiggins PA, Unrau PJ. 2014. RNA Mango aptamer-fluorophore: a bright, high-affinity complex for RNA labeling and tracking. *ACS Chem Biol* **9:** 2412–2420. doi:10.1021/cb500499x

Filonov GS, Moon JD, Svensen N, Jaffrey SR. 2014. Broccoli: rapid selection of an RNA mimic of green fluorescent protein by fluorescence-based selection and directed evolution. *J Am Chem Soc* **136:** 16299–16308. doi:10.1021/ja508478x

Gu J, Leszczynski J. 2002. Origin of Na^+/K^+ selectivity of the guanine tetraplexes in water: the theoretical rationale. *J Phys Chem A* **106:** 529–532. doi:10.1021/jp012739g

Hocine S, Raymond P, Zenklusen D, Chao JA, Singer RH. 2013. Single-molecule analysis of gene expression using two-color RNA labeling in live yeast. *Nat Methods* **10:** 119–121. doi:10.1038/nmeth.2305

Hud NV, Smith FW, Anet FAL, Feigon J. 1996. The selectivity for K^+ versus Na^+ in DNA quadruplexes is dominated by relative free energies of hydration: a thermodynamic analysis by ^{1}H NMR. *Biochemistry* **35:** 15383–15390. doi:10.1021/bi9620565

Jeng SCY, Chan HHY, Booy EP, McKenna SA, Unrau PJ. 2016. Fluorophore ligand binding and complex stabilization of the RNA Mango and RNA Spinach aptamers. *RNA* **22:** 1884–1892. doi:10.1261/rna.056226.116

Jeng SCY, Trachman RJ, Weissenboek F, Troung L, Link K, Jepsen MB, Knutson J, Andersen E, Ferré-D'Amaré AR, Unrau PJ. 2020. Fluorogenic aptamers resolve the flexibility of RNA junctions using orientation-dependent FRET. *RNA* doi: 10.1261/rna.078220.120.

Jepsen MDE, Sparvath SM, Nielsen TB, Langvad AH, Grossi G, Gothelf KV, Andersen ES. 2018. Development of a genetically

encodable FRET system using fluorescent RNA aptamers. *Nat Commun* **9:** 1–10. doi:10.1038/s41467-017-02088-w

Lane AN, Chaires JB, Gray RD, Trent JO. 2008. Stability and kinetics of G-quadruplex structures. *Nucleic Acids Res* **36:** 5482–5515. doi:10.1093/nar/gkn517

Lorsch JR, Szostak JW. 1994. In vitro selection of RNA aptamers specific for cyanocobalamin. *Biochemistry* **33:** 973–982. doi:10.1021/bi00170a016

Mujumdar RB, Ernst LA, Mujumdar SR, Lewis CJ, Waggoner AS. 1993. Cyanine dye labeling reagents: sulfoindocyanine succinimidyl esters. *Bioconjugate Chem* **4:** 105–111. doi:10.1021/bc00020a001

Paige JS, Wu K, Jaffrey SR. 2011. RNA mimics of green fluorescent protein. *Science* **333:** 642–646. doi:10.1126/science.1207339

Song W, Filonov GS, Kim H, Hirsch M, Li X, Moon JD, Jaffrey SR. 2017. Imaging RNA polymerase III transcription using a photostable RNA–fluorophore complex. *Nat Chem Biol* **13:** 1187–1194. doi:10.1038/nchembio.2477

Trachman RJ, Ferré-D'Amaré AR. 2019. Tracking RNA with light: selection, structure, and design of fluorescence turn-on RNA aptamers. *Q Rev Biophys* **52:** e8. doi:10.1017/S0033583519000064

Trachman RJ, Demeshkina NA, Lau MWL, Panchapakesan SSS, Jeng SCY, Unrau PJ, Ferré-D'Amaré AR. 2017. Structural basis for high-affinity fluorophore binding and activation by RNA Mango. *Nat Chem Biol* **13:** 807–813. doi:10.1038/nchembio.2392

Trachman RJ, Abdolahzadeh A, Andreoni A, Cojocaru R, Knutson JR, Ryckelynck M, Unrau PJ, Ferré-D'Amaré AR. 2018. Crystal structures of the Mango-II RNA aptamer reveal heterogeneous fluorophore binding and guide engineering of variants with improved selectivity and brightness. *Biochemistry* **57:** 3544–3548. doi:10.1021/acs.biochem.8b00399

Trachman RJ, Autour A, Jeng SCY, Abdolahzadeh A, Andreoni A, Cojocaru R, Garipov R, Dolgosheina EV, Knutson JR, Ryckelynck M, et al. 2019. Structure and functional reselection of the Mango-III fluorogenic RNA aptamer. *Nat Chem Biol* **15:** 472–479. doi:10.1038/s41589-019-0267-9

Trachman RJ, Cojocaru R, Wu D, Piszczek G, Ryckelynck M, Unrau PJ, Ferré-D'Amaré AR. 2020. Structure-guided engineering of the homodimeric mango-IV fluorescence turn-on aptamer yields an RNA FRET pair. *Structure* **28:** 776–785.e3. doi:10.1016/j.str.2020.04.007

Wu B, Chen J, Singer RH. 2014. Background free imaging of single mRNAs in live cells using split fluorescent proteins. *Sci Rep* **4:** 1–3. doi:10.1038/srep03615